Virtual screening and QSAR study of some pyrrolidine derivatives as α-mannosidase inhibitors for binding feature analysis

N. S. H. N. Moorthy [*],[†], Natércia F. Brás [†], Maria J. Ramos, Pedro A. Fernandes

REQUIMTE, Departamento de Química e Bioquímica, Faculdade de Ciências, Universidade do Porto 687, Rua do Campo Alegre, 4169-007 Porto, Portugal

ARTICLE INFO

ABSTRACT

Virtual screening and QSAR analysis were carried out to investigate the binding features of (2R, 3R, 4S)-2-aminomethylpyrrolidine 3,4-diol and the functionalized pyrrolidine derivatives to the α-mannosidase I and II enzymes. The QSAR models (possessed considerable R^2, Q^2 values, etc.) suggested that the presence of polar property on the vdW surface (vsurf_W, vsurf_Wp, etc.) of the molecules is important along with the presence of aromatic rings (opr_violation) in the molecules (which also provide hydrophobicity to the molecules). The docking study performed on α-mannosidase I and II enzymes pointed that the main interactions occur by hydrogen bonds, hydrophobic π–π stacking contacts and salt bridges with the cation calcium (for α-mannosidase I) and close interaction with zinc ion (α-mannosidase II), respectively. The bond flexibility orientates the aromatic ring in the molecules toward the hydrophobic cavity for π–π stacking contacts with the aromatic amino acids (Phe528, Phe329 and Phe659 for α-mannosidase I and Trp95, Tyr269, Phe312, Tyr102 for α-mannosidase II). The pharmacophore analysis also supports the results derived from the docking and QSAR studies. Our results suggest that the best compound to inhibit both classes of α-mannosidase is the compound **30**, which may be used to design similar and better inhibitors to next generation drugs.

1. Introduction

The glycosidase family enzymes such as glucosidases, glucotransferases, mannosidases, galactosidases, etc, work on the glycosylation pathway that cleave the glycosidic bond of the oligosaccharides and liberate glucose which causes the carbohydrate digestion and/or the biosynthesis of N-linked oligosaccharides. The maturation of N-linked oligosaccharides in mammalian cells starts with the transfer of an oligosaccharide precursor, $Glc_3Man_9GlcNAc_2$, to the nascent polypeptide chain entering the endoplasmic reticulum (ER).[1–3] This process is mediated by oligosaccharyltransferases, which recognize N-linked glycosylation sequences (Asn-X-Ser/Thr) in target proteins. Following this, α-glucosidases and α-mannosidases I (class I – EC3.2.1.113) in ER trim this oligosaccharide precursor to $Man_8GlcNAc_2$, and the glycoprotein is transported to Golgi apparatus, where the remaining α-linked mannose residues are removed by α-mannosidase II (class II – EC 3.2.1.114), resulting in the matured glycosylation structure on each glycoprotein destined for secretion, cell surface or lysosomes.[4–6]

Some disturbed specific carbohydrate structures on the cell surface are associated with diseases, cancer progression and metastasis. This altered distribution occurs due to the abnormalities in the N-glycosylation pathway, namely in α-mannosidase I and α-mannosidase II activities.[4,6] α-1,2-Mannosidase I and II belong to glycosyl hydrolases families 47 and 38, respectively. The former is calcium-dependent and cleaves α-1,2-linked mannose residues with inversion of anomeric configuration, while in class II enzymes, the zinc ion involves the catalytic reaction and retains the sugar anomeric configuration.[7–10] Consequently, both enzymes are key targets in the development of anticancer therapeutics.

Glycosyl hydrolases enzymes have high biological interest to medicinal chemists and pharmaceutical industries for the development of novel therapeutics for carbohydrate mediated diseases. Some molecular modelling, molecular docking, quantum mechanics and hybrid quantum mechanics/molecular mechanics (QM/MM) have been made on this group of enzymes.[11–22] Literatures revealed that Kuntz et al. worked on the binding mode analysis of α-mannosidase II enzyme inhibitors[23–25] and Sivapriya et al. reported their work on α-mannosidase I enzyme inhibitors.[26]

The combined analysis such as structure based drug design (docking), quantitative structure–activity relationship (QSAR) and pharmacophore analysis provide remarkable information on the structural feature of the inhibitors for the interaction and give guidance for the novel drug design. QSAR analysis is one of the techniques used to investigate the correlation between activities, (generally, biological activities) and the physicochemical

* Corresponding author.
E-mail addresses: hari.moorthy@fc.up.pt (N.S.H.N. Moorthy), pafernan@fc.up.pt (P.A. Fernandes).
† These authors equally contributed to this work.

properties of a set of molecules. This ranks the feature of the ligands that needed to interact with the active site residues.[15,27,28]

In this present work, we have performed a virtual screening study of various pyrrolidine derivatives (two sets of compounds carrying (2R, 3R, 4S)-2-aminomethylpyrrolidine 3,4-diol and functionalized pyrrolidine derivatives)[29,30] into the active site of both α-1,2-mannosidase I and II (α-1,2-mannosidase I in complex with kifunensine (KIF) and 1-deoxymannojirimycin (DMNJ) inhibitors, as well as α-1,2-mannosidase II bound to the potent inhibitors DMNJ and swainsonine (SWA))[7,31] to understand the molecular interactions between them. The structural analyses of these compounds were also carried out using QSAR techniques to elucidate the structural features of the molecules responsible for these interactions. From the literature, it confirms that our QSAR analysis is the first report on this target. In sum, the enzyme-inhibitor interactions studied here provide insight to the design of novel inhibitors of both α-mannosidase enzymes.

2. Material and methods

2.1. QSAR study

The reliability, robustness and predictability of the QSAR results depend on the selected data set, the method of statistical analysis and the validation of the developed models. The pyrrolidine derivatives possessed α-mannosidase inhibitory activity against the enzyme obtained from almond and jackbean was considered for this study (Tables 1–3).[29,30] Among the 30 compounds in the data set, only 26 and 20 compounds have defined inhibitory activity against jackbean and almond α-mannosidase enzymes, respectively. Hence, the remaining compounds in the data set have either no inhibition at the specified concentration or experimentally not determined were omitted from the analysis. α-Mannosidase inhibitory activity of the compounds reported as percentage inhibition were converted as pIC_{50} by log $(P/100-P)$, where P is the percentage inhibition.[14,15,17]

The molecular operating environment (MOE) software[32] was used to optimize the energy and the calculation of physicochemical descriptors of the molecules. The semi-empirical MOPAC program with Hamiltonian Austin Model 1 (AM1) force field with 0.05 RMS gradients of MOE software was used to optimize the molecules. A large number of theoretical molecular descriptors available in the package were calculated to define the structural property of the molecules[33] needed to perform QSAR analysis. The data set (with defined activity) was divided randomly as training set (70%) and test set (30%) for the correlation analysis using the Statistica 8.0 software.[34] Multiple linear regression (MLR) analysis was used to perform the study. The significant models selected were further undergone validation study by internal (LOO, LMO and Bootstrapping) and external (test set) methods.[35,36] Multicollinearity and serial autocorrelations of the descriptors and the models were tested with variance inflation factor (VIF) and Durbin–Watson (DW) values. The rule of thumb was adapted to select number of descriptors in the models (3–6 times the number of parameters under consideration).[37]

2.2. Docking study

2.2.1. Structures preparation and docking protocol

The X-ray crystallographic structures of α-mannosidase I (1FO2 and 1FO3 codes at 2.4 Å and 1.8 Å of resolutions)[7] and α-mannosidase II (1HWW and 1HXK codes at 1.9 Å and 1.5 Å of resolution)[31] were obtained from the Protein Data Bank. All crystallographic water molecules and ligands were removed to obtain the unbound structures of each enzyme. All hydrogen atoms were added, taking into account of all residues in their physiological protonation state. Structures of all pyrrolidine derivatives were built with GaussView 5.0 software.[38]

Ligand–protein docking was performed with the vsLab (virtual screening lab), an easy-to-use graphical interface for the molecular docking software AutoGrid/AutoDock that has been included into VMD as a plug-in.[39] AutoDock 4.2[40] was used for the docking calculations, and the program VMD 1.8.6[41] was used for visual inspection and analysis.

Kollman partial charges were assigned to all protein atoms, while for the zinc and calcium ions, formal charges of +2 were applied. The grid maps were centred next to ions and comprised $51 \times 51 \times 51$ points of 0.375 Å spacing. The Lamarckian genetic algorithm was employed with the following parameters: population size of individuals: 150; maximum number of energy evaluations: 2.5×10^6 and maximum number of generations: 27 000. For all the calculations, 50 docking rounds were performed with step sizes of 2.0 Å for translations and with orientations and torsions of 5.0°. Docked conformations were clustered within 2.0 Å root-mean-square-deviations (rmsd).
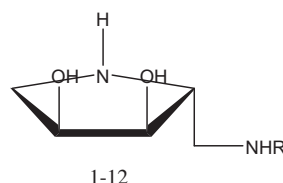
2.2.2. Pharmacophore analysis

The pharmacophore analysis of the data set was carried out using MOE software. The conformers of the data set was developed by stochastic search covering maximum number of conformers generated to 250, superpose RMSD to 0.15 and the fragment strain limit of 4 kcal/mol. The lowest energy conformers obtained from the stochastic search was aligned using ligand flexibility on MMFF94× force field with the energy cutoff of 10 for non-bonded interactions. The following properties have been calculated for the aligned structures: the strain energy (U), the mutual similarity score (F) and the value of the objective function (S) of each alignment. The aligned structure exhibits lower U, F and S values were considered for the pharmacophore analysis.

3. Results and discussions

MLR analysis performed between physicochemical descriptors of the pyrrolidine derivatives and the biological activities (jackbean and almond α-mannosidase inhibitory activities) provided significant models, which are given in Table 4. In this analysis, we have developed several models including and excluding test set compounds (only the training set and the complete set of compounds). The reason behind the analysis of complete set compound is that it can provide additional information on the active site property of the enzyme and to validate the training set models.

Models 1 and 2 are biparametric and triparametric regression equations respectively, developed with training set compounds and the α-mannosidase inhibitory activity (almond). The model 3 has been constructed with the jackbean α-mannosidase inhibitory activity using training set compounds as the models 1 and 2. The complete data set was used to develop remaining models (4 and 5) with the jackbean and almond α-mannosidase inhibitory activities, respectively. The selected models 1 and 2 from almond α-mannosidase inhibitory activity have significant statistical parameters such as correlation coefficient >0.9, F_{test} values have 0.01 confidence level and the t_{test} values are also significant. As the training set models (1 and 2), the complete set model 4 also has significant statistics. The models 3 and 5 are having acceptable statistical parameters compared with other models. The contributed physicochemical descriptors in all the models are different (also vdW surface area descriptors contributed efficiently in all models) and provided significant statistical parameters which confirms that the models are significant for further validation analysis.

Table 1
Structure and activity of the compounds used in the studies[29,30]

1-12

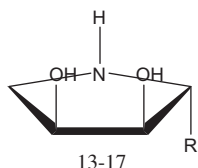| Comp No.	R	R₁	Percentage inhibition[a]	
			Almond	Jackbean
1	H		51	81
2	(CH(OH)CH₃, with OH dashed)		39	75
3	(CH(OH)CH₃, with OH wedge)		45	66
4	c-C₅H₉		53	60
5	(CH₂-piperidine NBn)		59	55
6	(CH₂-furan)		29	49
7	(CH₂-thiophene)		68	89
8	(CH₂-imidazole)		59	55
9	Bn		69	92
10	(C(Ph)(Ph)... CH₃, OH)		Ni	Ni
11	–CH(CH₃)Ph		48	66
12	–CH₂N(Ac)Bn		Ni	Ni

[a] Percentage of inhibitions at 1 mM concentration, pH :9.8, temperature: 35 °C, Substrate: *p*-nitrophenylglycoside, buffer: 0.2 M sodium borate buffer, enzyme concentration: 0.01–0.5 units/mL of enzyme (1 unit = 1 μmol of glycoside hydrolyzed/min).

The validation studies examine the self consistency and reliability of the models, which imply a quantitative assessment of the model robustness and its predictive power. The results derived from various validation methods are provided in Table 5. The training set models 1 and 2 show low standard error of predicted residual sum of squares (S_{PRESS}) (<0.2307) and standard deviation of the error of prediction (SDEP) (<0.2045 for training set and <0.1168 for test set) values, which revealed that the models 1 and 2 provided small residual values between observed and predicted activities. The model 3 also provides low S_{PRESS} and SDEP values for the training and test set compounds, however it is little higher than the values obtained from the models 1 and 2. The complete set models (model 4 and 5) have comparable S_{PRESS} and SDEP values, however the values are less than 0.4. The predicted residual sum of squares (PRESS) is another statistical parameter used to find out the residual error between the observed and the predicted activities. The models 1 and 2 have the PRESS values <0.58 and other models have

less than 2.6. This PRESS value has significant effect on the calculation of crossvalidated correlation coefficient (Q^2) of the models. The Q^2 value of models is one of the important parameters signify the predictive capacity of the models, which has been calculated from the PRESS values (Supplementary Tables S1 and S2).

The crossvalidated correlation coefficients (Q^2_{LOO}, Q^2_{LMO}, and Q^2_{BS}) of the derived models 1 and 2 are >0.7 for the training set compounds (almond α-mannosidase), while the complete set model (model 4) possessed poor Q^2 value (0.3545). The models developed with jackbean α-mannosidase inhibitory activity (both training set and complete set) have the Q^2 value >0.5. The test set compounds also provided significant Q^2 values >0.6 for all the models (models 1–3). The validation techniques provided significant results for the developed models. It may be considered that a high Q^2 (for instance $Q^2 > 0.5$) is one of the indicators, that the model is significantly predictive.[42,43] This reveals that the selected models have sufficient predictive power and self consistency.

Table 2
Structure and activity of the compounds used in the studies[29,30]

13-17

Comp No.	R	R_1	Percentage inhibition[a]	
			Almond	Jackbean
13	H		40	70
14	−CH₂OH		37	54
15	−CH(OH)CH₂OH		Ni	Ni
16	−CH₂CH₂NHPh		Ni	33
17	−CH₂CH(OH)₂		56	81

^a Percentage of inhibitions at 1 mM concentration, pH :9.8, temperature: 35 °C, substrate: *p*-nitrophenylglycoside, buffer: 0.2 M sodium borate buffer, enzyme concentration: 0.01–0.5 units/mL of enzyme (1 unit = 1 µmol of glycoside hydrolyzed/min).

The distance based approach also provides information on the stability of the models. The maximum Cook's distance values of the models are <0.0.5 which is <1 (squared Cook's distances)[44,45] except model 4. The compound 22 in the model 4 has little higher Cooks distance than 1. The structural information of the compounds showed that the compound 22 has a hydroxy methyl substituent on the pyrrolidine ring. Interestingly, this compound has higher inhibitory activity against both α-mannosidases (jackbean and almond). The Cook's distances of all the compounds have almost equal magnitude (<1), showing that the equation has significant predictive ability for the prediction of α-mannosidase inhibitory activities.
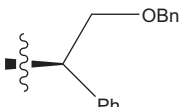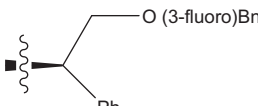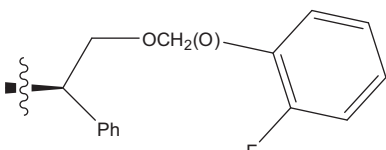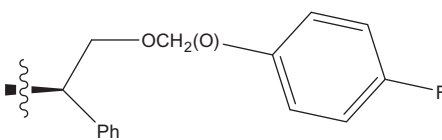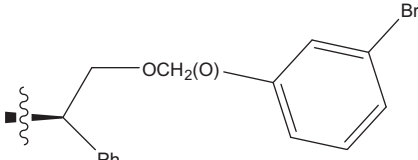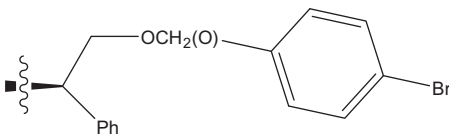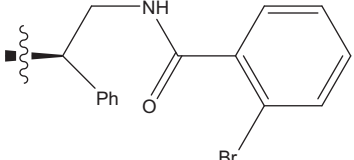
The multicolinearity and the autocorrelation of the models and the descriptors provide informations on the stability, reliability and robustness of the models. To confirm the absence of multicolinearity, the VIF value was calculated for each parameter in the regression equations. A VIF value greater than 10 is an indication of potential multicolinearity problems (inflated standard errors of regression coefficients). Not uncommonly, a VIF of 10 or even one as low as 4 (equivalent to a tolerance level of 0.10 or 0.25) have

Table 3
Structure and activity of the compounds used in the studies[29,30]

18-30
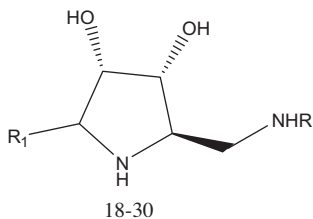
Comp No.	R	R_1	Percentage inhibition[a]	
			Almond	Jackbean
18		H	93	–
19		H	55	92
20		H	55	88
21		H	50	84
22			96	98
23		H	63	77

Table 3 (*continued*)

Comp No.	R	R$_1$	Percentage inhibition[a]	
			Almond	Jackbean
24	OBn, Ph	H	75	92
25	O (3-fluoro)Bn, Ph	H	Nd	99
26	OCH$_2$(O), Ph, F	H	Nd	83
27	OCH$_2$(O), Ph, F	H	Nd	92
28	OCH$_2$(O), Ph, Br	H	Nd	79
29	OCH$_2$(O), Ph, Br	H	Nd	92
30	NH, Ph, O, Br	H	Nd	89

[a] Percentage of inhibitions at 1 mM concentration, pH :9.8, temperature: 35 °C, Substrate: *p*-nitrophenylglycoside, buffer: 0.2 M sodium borate buffer, enzyme concentration: 0.01–0.5 units/mL of enzyme (1 unit = 1 μmol of glycoside hydrolyzed/min).

been used as rules of thumb to indicate excessive or serious multicolinearity.[46] In the selected models (training and complete set), the VIF values are less than 3 show that the descriptors in the selected models are free from multicolinearity, that is, none of the independent variables in the models are colinear with other independent variables in the model.[47] The results are provided in Supplementary Table S3.

A DW test was employed to check the serial correlation of residuals (correlation of adjacent residuals). If the DW statistic is substantially less than 2, there is evidence of positive serial correlation and a value toward 4 indicates negative autocorrelation.[48,49] The tabulated upper and lower bound values of DW were considered to test the hypothesis of zero autocorrelation against the positive and negative autocorrelations. In the present study, the DW values of both the models are higher than the tabulated upper and lower bound value at 5% significance level (Supplementary Table S3) and the values are closer to 2, show that the models are not having any serious autocorrelation problem.

The model 1 has developed between the α-mannosidase inhibitory activity (almond) and the physicochemical properties of the molecules. In this model, two vsurf_ descriptors such as vsurf_W2

and vsurf_Wp8 are contributed for the activity prediction. The vsurf_ descriptors are volume, surface properties depend on the structural connectivity and the conformation (dimensions are measured in Å) of the molecules.[50] These descriptors explain the interaction of molecules with hydrophobic and hydrophilic part of the protein through some surface properties such as shape, electrostatic, hydrogen-bonding and hydrophobicity. The vsurf_W descriptor explains the hydrophilic region of the molecules and are calculated at eight different energy levels (−0.2, −0.5, −1.0, −2.0, −3.0, −4.0, −5.0 and −6.0 kcal/mol) which may be defined as the molecular envelope accessible by solvent water molecules. The volume of this envelope varies with the level of interaction energies between the water and the solute molecules. In general, W1–4 account for polarizability and dispersion forces, while W5–8 account for polar and hydrogen bond donor-acceptor regions.[33,50] Here, the vsurf_W2 has calculated at −0.5 kcal/mol energy levels and the positive contribution of this descriptor explains that the polarizable property on the van der Waals (vdW) surface of the molecules is important for the interactions.

The vsurf_Wp descriptor describes the polar volume of the molecule and are calculated at eight different energy levels (−0.2,

Table 4
QSAR results derived from the present analysis

| Model No.	Model description	Statistical parameters
Model 1	$pIC_{50\ (Almond)}$ = 0.4355(±0.0814) vsurf_Wp8 + 0.0021(±0.0008) vsurf_W2 − 1.2237(±0.4100)	N = 14, R = 0.9384, R^2 = 0.8806, $AdjR^2$ = 0.8589, $F_{(2,11,0.01)}$ = 40.5660(7.206), SEE = 0.1853, $t_{(11,0.01)}$ = −2.9840(2.7181), p = 0.0124
Model 2	$pIC_{50\ (Almond)}$ = 5.1575(±1.5216) BCUT_PEOE_3 + 0.8047(±0.0659) vsurf_Wp8 −0.1602(±0.0267) vsurf_Wp7−14.5546(±4.3416)	N = 14, R = 0.9787, R^2 = 0.9579, $AdjR^2$ = 0.9453, $F_{(3,10,0.01)}$ = 75.8990(6.552), SEE= 0.1154, $t_{(10,0.005)}$ = −3.3520(3.1693), p = 0.0073
Model 3	$pIC_{50\ (Jackbean)}$ = 0.0043(±0.0015) vsurf_W3-0.1238(±0.0389) E_ang −4.6366(±1.0733) PEOE_VSA_FPOS + 3.9294(1.1585)	N = 18, R = 0.8313, R^2 = 0.6911, $AdjR^2$ = 0.6249, $F_{(3,14,0.01)}$ = 10.4430(5.564), SEE = 0.3331, $t_{(14,0.005)}$ = 3.3917(2.9768), p = 0.0044
Model 4	$pIC_{50\ (Almond)}$ = 0.4009(±0.1139) opr_violation −0.0379 (±0.0174) SMR_VSA3−1.3097(±0.2836) vsurf_EDmin3−1.7037(±0.3992)	N = 20, R = 0.8041, R^2 = 0.6466, $AdjR^2$ = 0.5803, $F_{(3,16,0.01)}$ = 9.7576(5.292), SEE = 0.2759, $t_{(16,0.0005)}$ = −4.2680(4.0150), p = 0.0006
Model 5	$pIC_{50\ (Jackbean)}$ = 0.0048(±0.0008) vsurf_W2−0.0626(±0.0118) SlogP_VSA0−0.3531(±0.1256) a_nO + 229.6017(±60.5332) GCUT_SLOGP_0 + 514.5934(±136.0104)	N = 26, R = 0.8718, R^2 = 0.7600, $AdjR^2$ = 0.7143, Q^2 = 0.658, $F_{(4,21,0.01)}$ = 16.6250(4.369), SEE = 0.2867, $t_{(21,0.005)}$ = 3.7835(2.8314), p = 0.0011

Table 5
Summary of the validation study

Parameters		Model 1 (Almond)	Model 2 (Almond)	Model 3 (jack)	Model 4 (Almond-complete)	Model 5 (Jack-complete)
R^2		0.8806	0.9579	0.6911	0.6466	0.7600
R^2_{test}		0.8678	0.7596	0.8314	—	—
Q^2_{LOO}		0.8149	0.9274	0.4943	0.3545	0.658
Q^2_{LMO}		0.8238	0.9182	0.5576	—	—
Q^2_{BS}		0.7398	0.9219	0.5800	—	—
Q^2_{test}		0.8279	0.652	0.6389|	—	—
PRESS		0.5855	0.2297	2.5467	2.2242	2.4606
$PRESS_{(test)}$		0.0404	0.0818	0.7590	—	—
S_{PRESS}		0.2307	0.1516	0.4265	0.3728	0.3423
SDEP		0.2045	0.1281	0.3761	0.3335	0.3076
$SDEP_{(test)}$		0.0820	0.1168	0.3080	—	—
R^2_{pred}		0.9096	0.8171	0.6537	—	—
Cooks	Min.	0.0005	0.0000	0.0005	0.0008	0.0000
	Max.	0.5052	0.2921	0.2718	1.0215	0.1758
	Avg.	0.0852	0.0766	0.0718	0.1048	0.0388

−0.5, −1.0, −2.0, −3.0, −4.0, −5.0 and −6.0 kcal/mol) as the vsurf_W descriptor.[33,50] The interaction energies between water and the solute molecules determine the polar volume of the molecules. In general, Wp1–4 account for polarizability and dispersion forces, while Wp5–8 account for polar and hydrogen bond donor-acceptor regions.[33,50,51] In the present model, the vsurf_Wp8 has contributed with positive sign proposes that the molecules should have considerable hydrogen bond donor and acceptor groups on the vdW surface for interaction with the target or water molecules present in the target.

The model 2 has been developed by using vsurf_ descriptors and an adjacency and distance matrix descriptor (BCUT_PEOE_3), in which the BCUT metrics are an extension of Burden's parameters. These are based on a combination of the atomic number for each atom and a description of the nominal bond-type for adjacent and non-adjacent atoms, and incorporate both connectivity information and atomic properties (e.g., atomic charge, polarizability, hydrogen bond abilities) relevant to intermolecular interactions.[52,53] The Burdeńs parameter BCUT_PEOE_3 has a BCUT descriptor that uses the atomic contribution to each ij entry of the adjacency matrix takes the value $1/\sqrt{b_{ij}}$ where b_{ij} is the formal bond order between bonded atoms i and j. The diagonal takes the value of the PEOE partial charges. The resulting eigenvalues are sorted and the smallest, 1/3-ile, 2/3-ile and largest eigenvalues are reported.[33,54,55] In the present model, the positively contributed descriptor, BCUT_PEOE_3 has sorted as 2/3-ile eignevalue and recommends that the bonds separated by small distance are important for the interactions. The importance of other descriptors contributed in the model (vsurf_WP7 and vsurf_WP8) is discussed already in the model 1.

The model 3 obtained from the MLR analysis between the α-mannosidase inhibitory activity (from jackbean) and the physicochemical descriptors. In this model, different type of physicochemical descriptors such as partial charge (PEOE_VSA_ FPOS) and potential energy (E-ang) alongwith surface area, volume and shape descriptors (vsurf_W3) contributed for the activity prediction. The significance of the vsurf_W descriptor has explained in earlier models. But this descriptor (vsurf_W3) has calculated at −0.5 kcal/mol energy level and explains the role of polarizability and dispersion forces for the interaction.[33,51] The positive contribution of this descriptor as other vsurf_W descriptors in earlier models illustrates that the polar property in the molecules has better interaction with the active site.
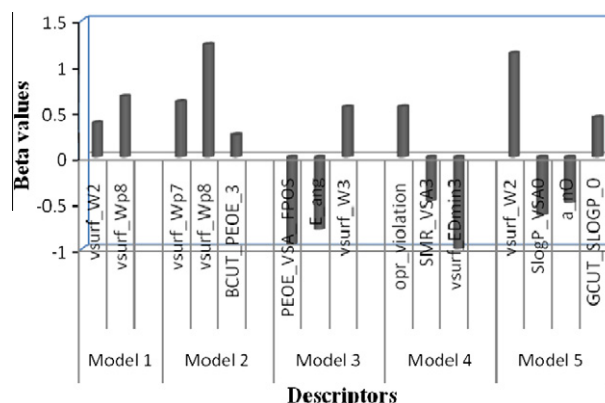
Figure 1. Contribution of descriptors present in the models for activity prediction.
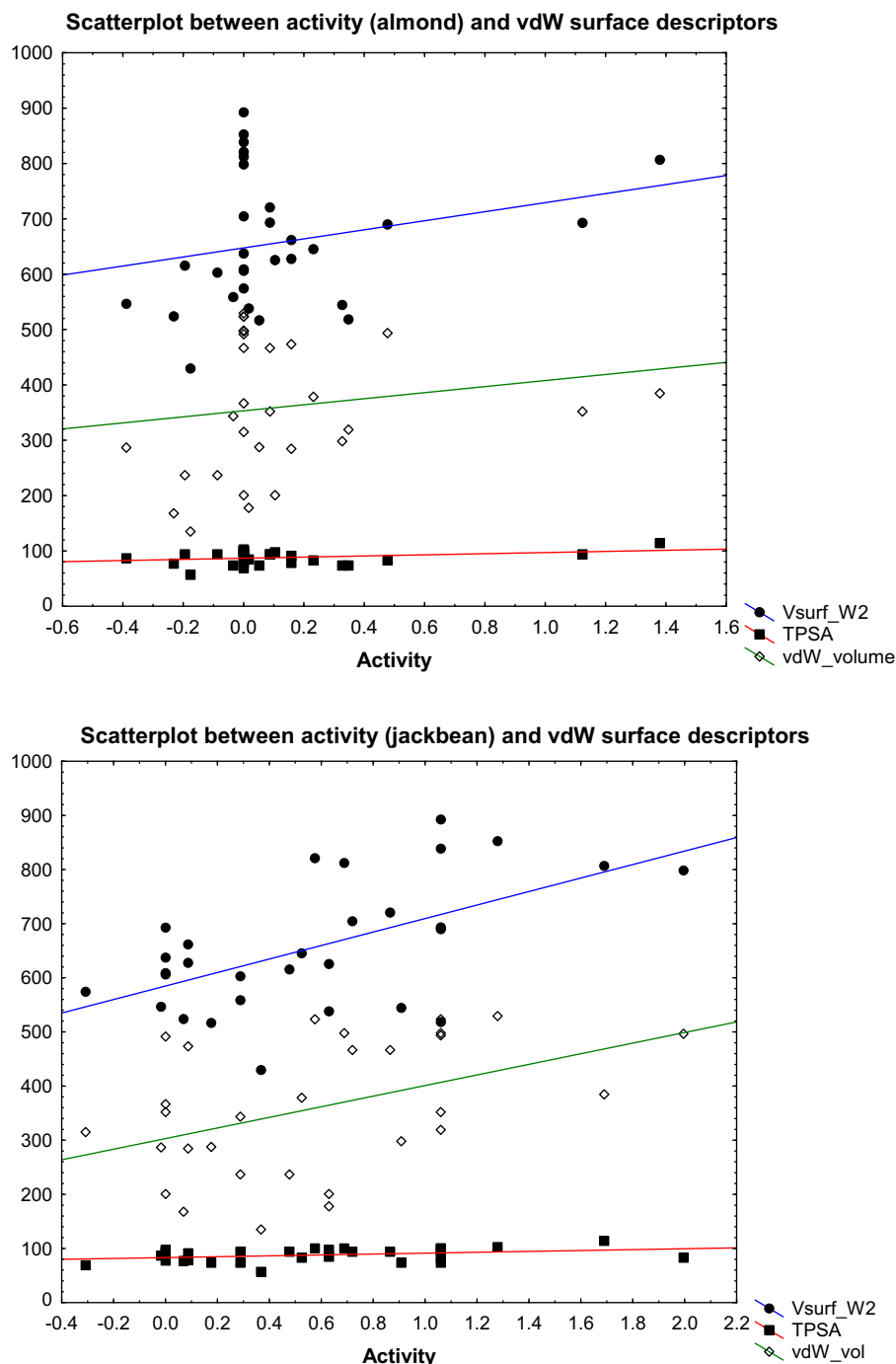
Scatterplot between activity (almond) and vdW surface descriptors

Scatterplot between activity (jackbean) and vdW surface descriptors

Figure 2. Scatterplot between the vdW and Opera properties and the biological activities.

The partial charge descriptor (PEOE_VSA_FPOS) present in model 3 describes the fractional positive vdW surface area. This is the sum of the v_i such that q_i is non-negative divided by the total surface area. The v_i are calculated using a connection table approximation.[33] Negative sign in this descriptor suggests that the fractional positive charge on the vdW surface of the molecule is detrimental for the activity. The other descriptor contributed in model 3 is E_ang, which explains the angle bend potential energy. This descriptor has contributed negatively in the model and which explains that the angle bend energy of the molecule should be low for better activity. It can be obtained if any molecule has flexible groups in their structure, which orientate towards the active site with less bending energy.

The model 4 developed with opr_violation, SMR_VSA3 and vsurf_EDmin3 descriptors. The opr_violation descriptor explains the number of violations of Oprea's lead-like test. As per the literature published by Opera, the property distribution of drug related chemicals depend upon number of rings (RNG), rigid bonds (RGB) and number of rotatable bonds (RTB) along with Lipinski parameters. The positive contribution of this descriptor explains that the compounds in the data set obeyed the Oprea's lead like test.[54] However, it explains that the rotatable bonds in the molecules are important for the inhibitory activity along with the polar properties.

SMR_VSA3 is defined to be the sum of the v_i for over all atoms i. p_i denotes the contribution to molar refractivity for atom i as

Scatterplot between activity (almond) and Oprea`s descriptors

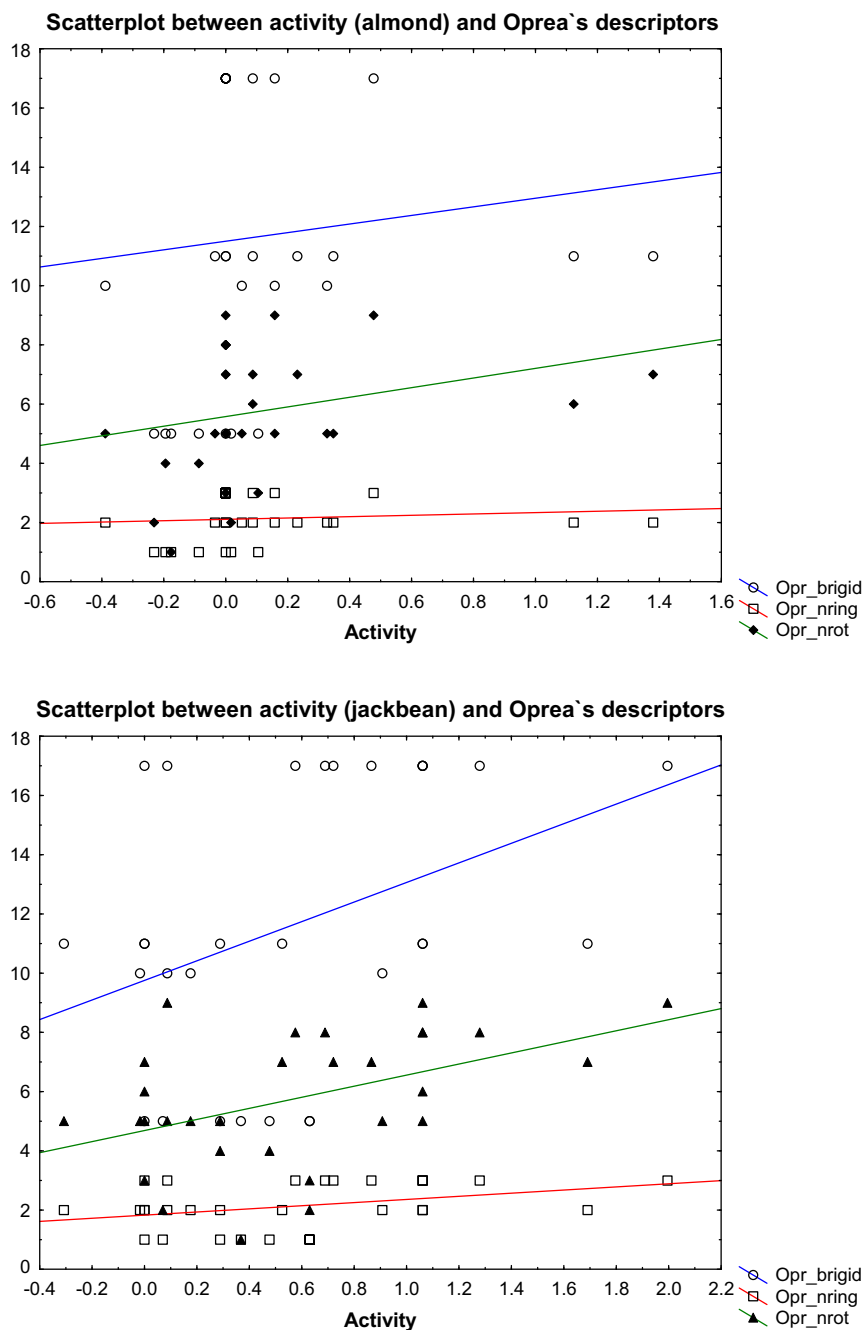Scatterplot between activity (jackbean) and Oprea`s descriptors

Fig. 2. (continued)

calculated in the SMR descriptor, calculated in a specified range, from 0.35 to 0.39. This descriptor intends to reflect the polarizability and the atomic contribution to the molar refractivity.[33,55] The negative sign of the regression coefficient in this descriptor suggests that the polarizability property on the vdW subdivided surface area of the molecule should be optimum for the favourable inhibitory activity. This reveals that the active site of the enzyme may have some distributed polarisable groups on the surface for better interaction.

Vsurf_Edmin3 describes the lowest hydrophobic energy and it represents the energies of interaction in kcal/mol, for the OH_2 and DRY probes of the best three local minima of interaction energy between the probe and the target molecule. The negative coefficient of this descriptor signifies the adverse effect of hydro-

phobic property of these molecules for the interactions. The subdivided surface area descriptors describe an approximate accessible vdW surface area (in Å^2) calculation for each atom, v_i, along with other atomic property, p_i (partition coefficient or molar refractivity). $SlogP\_VSA0$ defined to be the sum of the v_i for over all atoms i (calculated with $L_i > -0.4$) and the atomic property p_i ($logP$) for atom i as calculated in the $SlogP$ descriptor (calculated with the Wildman and Crippen $SlogP$ method).[33,56] The positive contribution of this descriptor reveals that the partition coefficient on the vdW surface of the molecule is favourable for the α-mannosidase inhibitory activity. The other descriptor, a_nO describes the number oxygen atoms in the molecules. In this model, this descriptor suggests that the presence of oxygen atom is unfavourable for the inhibitory activity showed that the number of oxygen atoms

Table 6
Docking results of the inhibitors studied into the X-ray structures of both α-mannosidase I and α-mannosidase II enzymes

ER α-Mannoidase Class I			Golgi α-Mannoidase Class II		
Inhibitor	$\Delta G_{binding}$ (kcal/mol)	K_i (μM)	Inhibitor	$\Delta G_{binding}$ (kcal/mol)	K_i (μM)
30	−9.27	0.16	30	−7.31	4.35
24	−9.05	0.23	27	−7.08	6.47
29	−8.89	0.31	20	−6.97	7.77
28	−8.88	0.31	25	−6.87	9.14
27	−8.68	0.44	26	−6.75	11.27
25	−8.35	0.76	22	−6.72	11.8
20	−8.33	0.79	28	−6.67	12.81
26	−8.24	0.91	29	−6.56	15.48
21	−7.61	2.62	21	−6.26	25.9
19	−6.71	12.04	18	−6.23	26.93
23	−6.71	12.14	19	−6.17	29.88
5	−6.66	13.08	23	−6.06	35.98
18	−6.51	16.81	5	−5.95	43.15
22	−6.29	24.55	12	−5.71	64.91
10	−6.23	27.14	24	−5.68	68.27
11	−6.22	28.10	10	−5.58	80.85
9	−6.08	35.02	11	−5.51	82.35
12	−5.93	44.84	16	−5.33	123.03
4	−5.69	66.91	9	−5.21	152.47
16	−5.63	74.31	15	−4.97	229.38
7	−5.61	77.66	7	−4.96	232.80
6	−5.27	136.13	6	−4.82	292.02
17	−4.83	286.85	4	−4.74	332.95
8	−4.76	325.87	17	−4.58	437.72
15	−4.54	168.79	2	−4.57	450.36
3	−4.52	487.86	13	−4.47	530.61
2	−4.14	918.32	8	−4.43	567.64
14	−3.95	1.26	3	−4.32	683.00
1	−3.82	1.59	1	−3.93	1310.00
13	−3.40	3.24	14	−3.88	1430.00

in the molecule should be optimum to maintain the hydrophilicity of the molecules. The significance of the descriptor, vsurf_W2 has been discussed earlier.

The GCUT descriptors are calculated from the eigenvalues of a modified graph distance adjacency matrix.[33,56] The GCUT_SLOGP_0 descriptors used atomic contribution to log$P$ (using the Wildman and Crippen Slog$P$ method) instead of partial charge. The positive contribution of the descriptor reveals that the presence of optimum hydrophobicity on the vdW subdivided surface of the molecules is important for the activity.

The relative contribution of each descriptor in the models for the activity prediction is provided in Figure 1. This figure explains that the vdW surface area properties (including vsurf_ descriptors) have contributed efficiently for the activity prediction. The descriptors in the models obtained for the almond and the jackbean α-mannosidase inhibitory activity showed that the polar property including vdW surface properties significantly contributed in the almond α-mannosidase inhibitory activity. The hydrophobic properties along with some polar properties contributed for the jackbean α-mannosidase inhibitory activity prediction. These reveal that the active site environment of both the enzymes may have little variation by the presence of some hydrophobic amino acids (may be aromatic amino acid residues), which causes the variation in activity. It pointed that the active site of the almond enzyme may have hydrophilic environment due to the presence of polar amino acids. The descriptors present in the models obtained from the α-mannosidase enzymes (almond) may be different, but provide information on the importance of the hydrophilic properties (hydrogen bonding) for the activity. It is interesting that the compounds containing acyclic side chain possessed less inhibitory effect against almond α-mannosidase enzymes. It also showed that the presence of aromatic rings have significant activity which confirms that the active site of the enzyme should have some aromatic

amino acids for the π–π stacking interactions with the aromatic rings in the molecules.

In order to describe the activity space with respect to the physicochemical properties, we have made scatterplot between the activities (almond and jackbean) and the volume, surface properties (vsurf_W2, TPSA and vdW_vol) and the Oprea's descriptors (Opr_nring, Opr_brigid and Opr_nrot) (Fig. 2). The figures showed that the almond α-mannosidase inhibitory activity has increased with rises in vsurf_W2 and TPSA values, while the vdW volume of those compounds are decreased. Some compounds possessed small vdW_vol, but possessed low α-mannosidase inhibitory activity values may caused by lower vsurf_W2 values. It is interesting to note that some inactive compounds has higher vsurf_W2 and TPSA values, but possess no α-mannosidase inhibitory activity, may be due to the higher vdW_vol values. The figure for Opera descriptors showed that average number of rings, rotatable bonds and rigid bonds has significant activities. It explains that the compounds have 17 (rigid bonds), 9 (rotatable bonds) and 3 (rings) possessed unfavourable effect on the inhibitory activity, while 11 (rigid), 6 (rotatable) and 2 (rings) exhibited significant activities. The increased numbers of rings cause hydrophobicity to the molecules which reduce the overall polar properties of the molecules.

The jackbean α-mannosidase inhibitory activity of the compounds showed that increased ring and rigid bonds have favourable effect on the α-mannosidase inhibitory activity. The number rotatable bonds in the molecules also play an important role with these properties. Unlike the inhibitory activity on almond α-mannosidase enzyme, the descriptors are distributed in the plot area against the jackbean α-mannosidase inhibitory activity. In comparison, the jackbean α-mannosidase inhibitory activity depends upon the increased vdW volume of the compounds along with other vdW surface properties than the almond α-
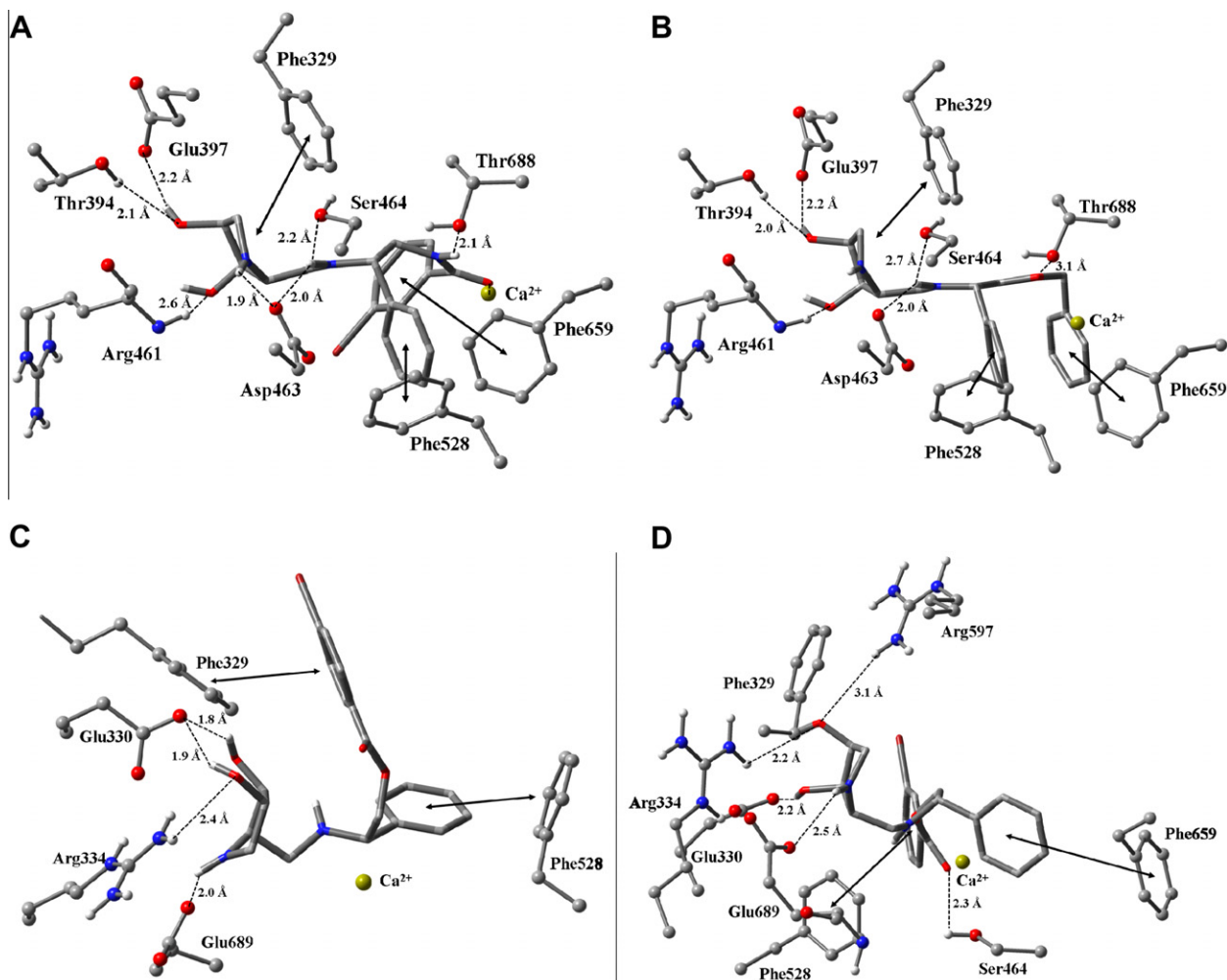
Figure 3. Interactions established by the amino acids of α-mannosidase I enzyme to the best four-ranked inhibitors: (A) compound 30, (B) compound 24, (C) compound 29 and (D) compound 28.

mannosidase inhibitory (in almond, the vdW volume should be medium). These graphs explain that the vdW volume and increased number of rings are favourable for the jackbean α-mannosidase inhibitory activity. These properties may provide additional hydrophobic property for the molecules for better inhibitory activity.

3.1. Virtual screening studies

Virtual screening study was carried out on the pyrrolidine derivatives against the α-mannosidase I and II enzymes. The experimental activities reported for the molecules are against the almond and jackbean α-mannosidase enzymes. The QSAR studies on those compounds interpreted some structural features of the active site of almond and jackbean α-mannosidase enzymes. Further, in order to investigate the binding interactions of those molecules on human α-mannosidase enzymes, we have performed virtual screening of those molecules against human α-mannosidase I and Golgi α-mannosidase II enzymes.

Initially, we have performed docking of the well known inhibitors KIF and DMNJ to the α-mannosidase I active site, as well as the DMNJ and SWA inhibitors to the α-mannosidase II active site to validate the docking study. The RMSD values of the best five predicted docking solutions to the crystallographic position of each inhibitor were used to evaluate our results. The average RMSD values obtained for α-mannosidase I complex with KIF

and DMNJ inhibitors, as well as α-mannosidase II complex with DMNJ and SWA drugs were 0.974 ± 0.003 Å and 0.822 ± 0.003 Å, 0.866 ± 0.019 Å and 0.468 ± 0.001 Å, respectively. All these small values reveal that our protocol have higher ability to predict the binding mode of inhibitor into the active site of α-mannosidase enzyme. The docking parameters used for the binding mode and affinity studies of the known compounds were applied for the docking study of all pyrrolidine derivatives. The binding energy and inhibitory constant values obtained for all compounds studied are shown in Table 6. We have performed a ranking of all compounds based on the binding energy values for further discussion.

3.2. α-Mannosidase I

The docking results derived for the pyrrolidine derivatives against the α-mannosidase I enzyme are provided in Table 6. Among the inhibitors, four top-ranked inhibitors (30, 24, 29 and 28) are considered in the discussion and to simplify our results. The representations and the most important interactions of the molecules established with the enzyme are summarized in Figures. 3 and 4. As noticed, the compound 30 is the one that establish more contacts with the enzyme binding pocket. It connected to the structural calcium by its carbonyl oxygen and the hydroxyl groups in the pyrrolidine nucleus establish several hydrogen bonds with the amino acid residues such as Thr394, Glu397 and Arg461.
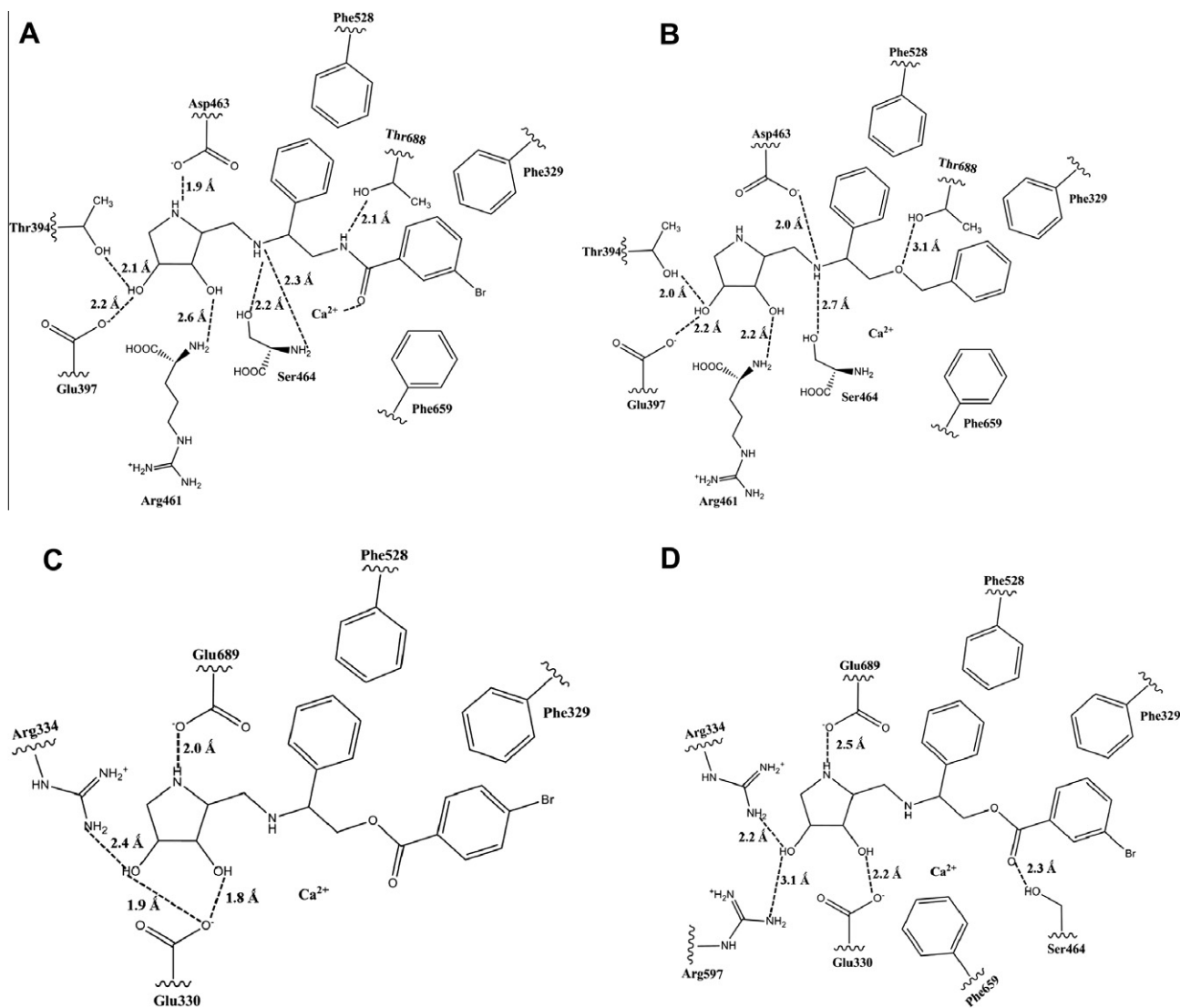
Figure 4. Representation of the interactions established by the amino acids of α-mannosidase I enzyme to the best four-ranked inhibitors: (A) compound 30, (B) compound 24, (C) compound 29 and (D) compound 28.

Other hydrogen bridges were also established between the NH groups of the molecules and the hydrophilic amino acids (Asp463, Ser464 and Thr688). The Phe528 moiety and the benzyl ring display several vdW interactions, whilst the Phe329 and Phe659 side chains make T-shaped π–π stacking contacts with its bromobenzene group. Analyzing the interactions occurred with the compound 24, it was verified that the non-availability of the carbonyl group in this compound disallows its interaction with the calcium cation, which is probably the reason for its weakest binding energy when compared with the previous compound 30. The experimental studies against the jackbean and almond α-mannosidase enzymes showed that this compound has higher activity than other compounds. However, hydrogen bonds were also observed between the compound 24 and the Thr394, Glu397, Arg461, Ser464 and Thr688 residues. Hydrophobic contacts also occur between the Phe329, Phe528 and Phe659 residues to the aromatic rings of inhibitor 24. Similar binding mode and contacts were established with the enzyme and the inhibitor 28, which is ranked in the fourth position. These results pointed that the overall conformations of inhibitors 30, 24 and 28 are similar, but the other compound (29) provided different binding mode than earlier compounds. This compound only makes hydrogen bonds with the

Glu332, Arg336 and Glu689 amino acids and their benzyl rings have vdW contacts with the side chain of Phe329 and Phe528 residues. However, the binding energy values and binding pose of these four inhibitors are very similar (a difference of 0.39 kcal/mol between the binding energies of the first and fourth compounds), revealing that these amino acids are important for the interaction.

These obtained results coincide with a research work reported by Supriya et al.[26] for thiosugar derivatives on α-mannosidase I enzyme interaction. They showed that Thr688, Glu663, Asp 463, Ser464 and Glu602 have interactions with the thiosugar moieties. There are a few catalytic amino acid residues like Thr688, Asp463 and Ser464, which bind to all the studied ligands through hydrogen bonding. The aminoacid residue Ser464 also makes vdW interaction with the studied molecules. These results confirm that the developed docking models of the pyrrolidine derivatives express the same binding mode as reported on the thiosugar moieties. Therefore, the most important residues of the α-mannosidase I enzyme are the Phe329, Thr394, Glu397, Arg461, Ser464, Phe528, Thr688 and Phe659, as well as the structural calcium ion. These aromatic amino acid residues form a hydrophobic cavity for the π–π stacking interaction with the aromatic rings in the molecules

6956

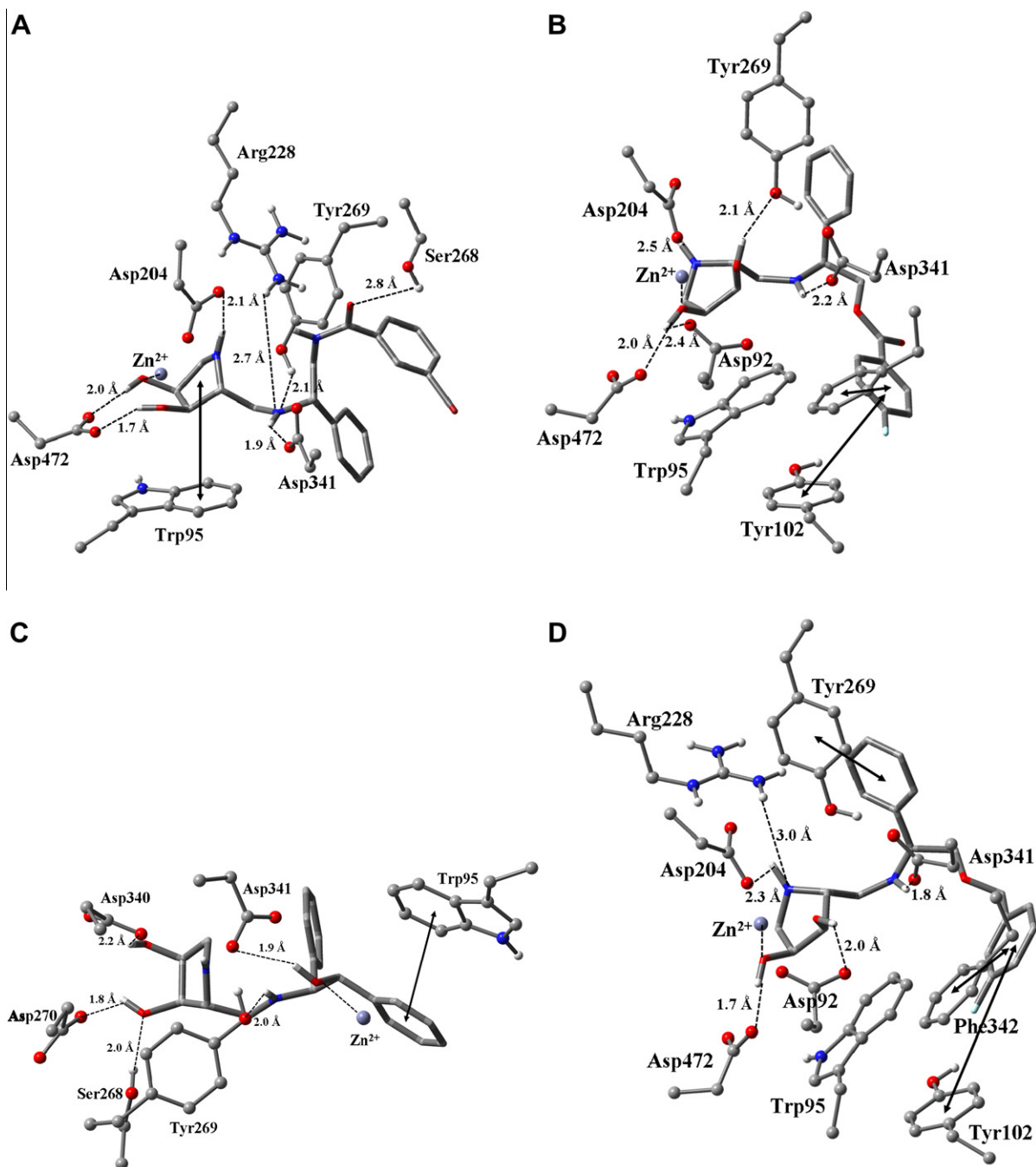*N. S. H. N. Moorthy et al. / Bioorg. Med. Chem. 20 (2012) 6945–6959*

Figure 5. Interactions established by the amino acids of α-mannosidase II enzyme to the best four-ranked inhibitors: (A) compound 30, (B) compound 27, (C) compound 20 and (D) compound 25.

and the glutamic and aspartic acid residues provide acidic/hydrophilic environment for hydrogen bonding with the polar part of the molecules.

3.3. α-Mannosidase II

The binding energy values obtained from the docking studies given in Table 6 provides four best inhibitors (30, 27, 20 and 25). Figures 5 and 6 show the interactions established between these compounds and the amino acids present in the binding pocket of α-mannosidase II enzyme. Similar to the α-mannosidase I inhibition, the compound 30 is also established better interactions with

the α-mannosidase II enzyme. As seen, its carbonyl group makes a hydrogen bond with the Ser268 residue, while the NH groups establish hydrogen bonds with the Asp204, Arg228, Tyr269 and Asp341 residues. One hydroxyl group in the pyrrolidine moiety makes a hydrogen bridge with the carboxyl group of the Glu472 residue and the oxygen atom of the other OH group interacts with zinc ion. In addition, the benzene ring possesses π–π stacking contacts with the aromatic side chain of Trp95 amino acid. The second-ranked inhibitor (27) exhibits mainly hydrophobic contacts with the enzyme, in particular with the aromatic side chains of Trp95, Tyr102, Tyr269 and Phe342 residues. The hydrophilic NH and OH groups also make hydrogen bonds with the Asp92,
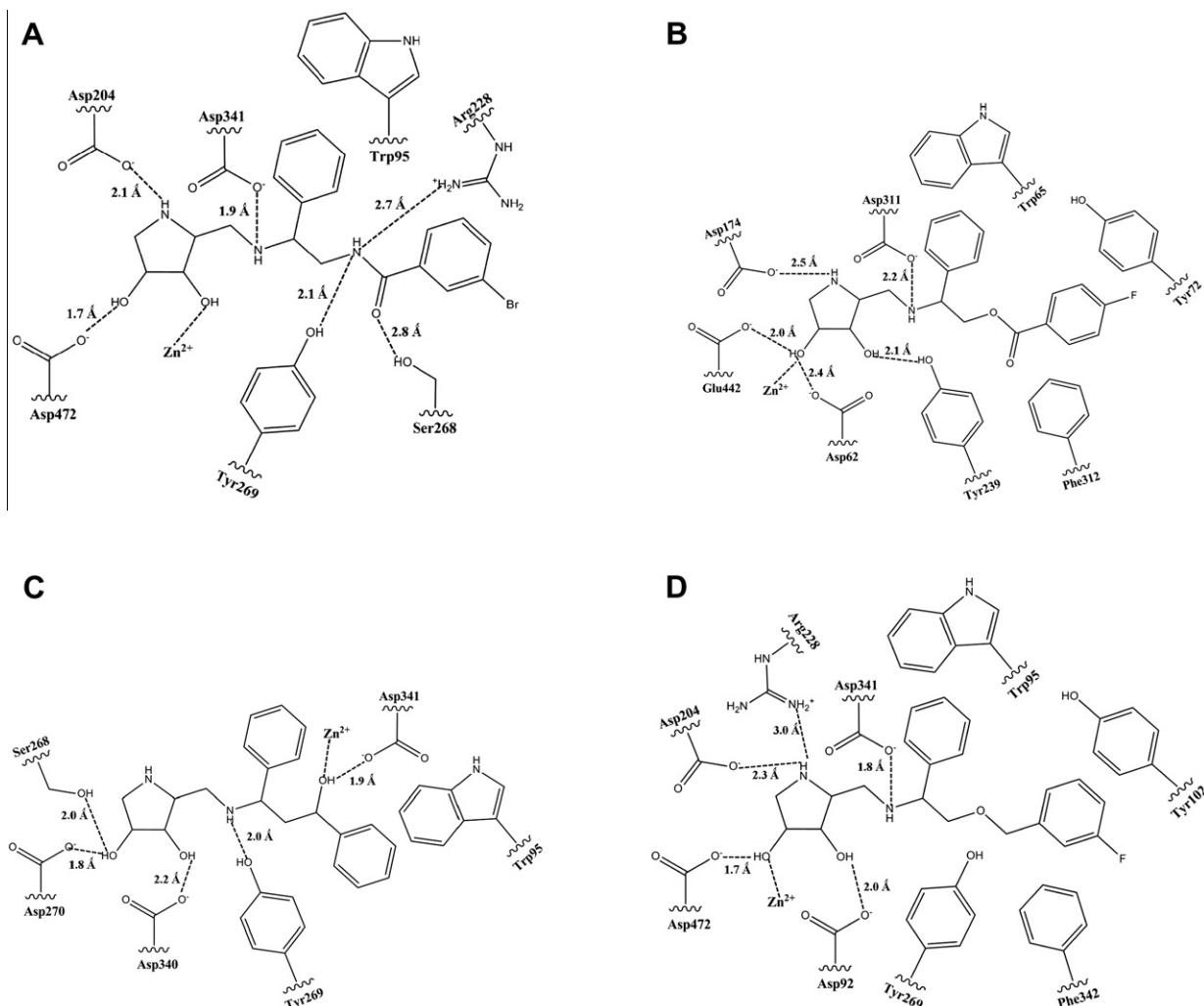
Figure 6. Representation of the interactions established by the amino acids of α-mannosidase II enzyme to the best four-ranked inhibitors: (A) compound 30, (B) compound 27, (C) compound 20 and (D) compound 25.

Asp204, Tyr269 and Asp341. The oxygen atom of one hydroxyl group in pyrrolidine moiety also stabilizes the positive charge of the zinc ion. The other two compounds (20 and 25) show similar interactions with the α-mannosidase II active site, which agree with the proximity of their binding mode conformations and binding energies values (a difference of 0.44 kcal/mol between the binding energies of the first and fourth compounds).

We have compared our results with the published reports. Kuntz et al., have worked on the binding mode analysis of α-mannosidase inhibitors on *Drosophila* Golgi α-mannosidase II enzyme. Studies conducted with SWA and DMNJ provide a large contribution of hydrophobic interactions involving aromatic residues Trp95, Phe206 and Tyr727, form hydrophobic cavity. The aromatic ring of the inhibitors π–π stacked with Trp95 and the polar part of the molecules form hydrogen bonds with the zinc ion.[24,57] The interaction analysis of mannostatin A to the enzyme reveals that the crucial contribution of zinc interactions and interactions with Asp341 and Asp472, as well as the water are important for the inhibitor binding. They also illustrated the importance of the interaction to the Arg876 backbone carbonyl as well as hydrophobic interactions with Phe206, Trp415 and Tyr727 as additional contributory factors for the mannostatin A inhibitory activity.[23,58] A research work reported by the same research group on pyrrolidine derivatives using different docking

programs suggested that five residues (Tyr727, Trp95, Arg228, Tyr269 and Asp92) in the flexible protein, moves of about 1 Å for specific atoms were observed with different programs. The location of the zinc atom also varied in each case. The docking result of one of the compounds illustrated that the phenyl group of the compound was predicted to interact with Arg228 through π interactions, while it was involved in a T-shaped π interaction with Trp95 in the crystal structure.[25]

The literature reports validate the results of our present study that the hydroxyl groups in the pyrrolidine ring (30, 27 and 25) form hydrogen bonding with the Asp472, Asp92 and Asp204 residues and zinc ion. The compound 20 has hydrogen bonding with Ser268, Asp240 and Asp340. As mentioned by the reported works, the Trp95 plays important role for the aromatic interaction with the phenyl rings in the compounds. The aromatic amino acids such as Trp95, Tyr269, Phe342 and Tyr102 form hydrophobic cavity for the phenyl ring interactions. Arg228 plays a role for the interaction with the nitrogen atom in the pyrrolidine ring or other nitrogen atoms in the molecules.

Therefore, the main hydrophilic amino acids those contribute to an efficient inhibitor binding are the following: Asp92, Asp204, Arg228, Ser268, Tyr269, Asp270, Asp340, Asp341 and Asp472; whilst the crucial aromatic residues the π–π stacking interactions are Trp95, Tyr102, Tyr269 and Phe342.
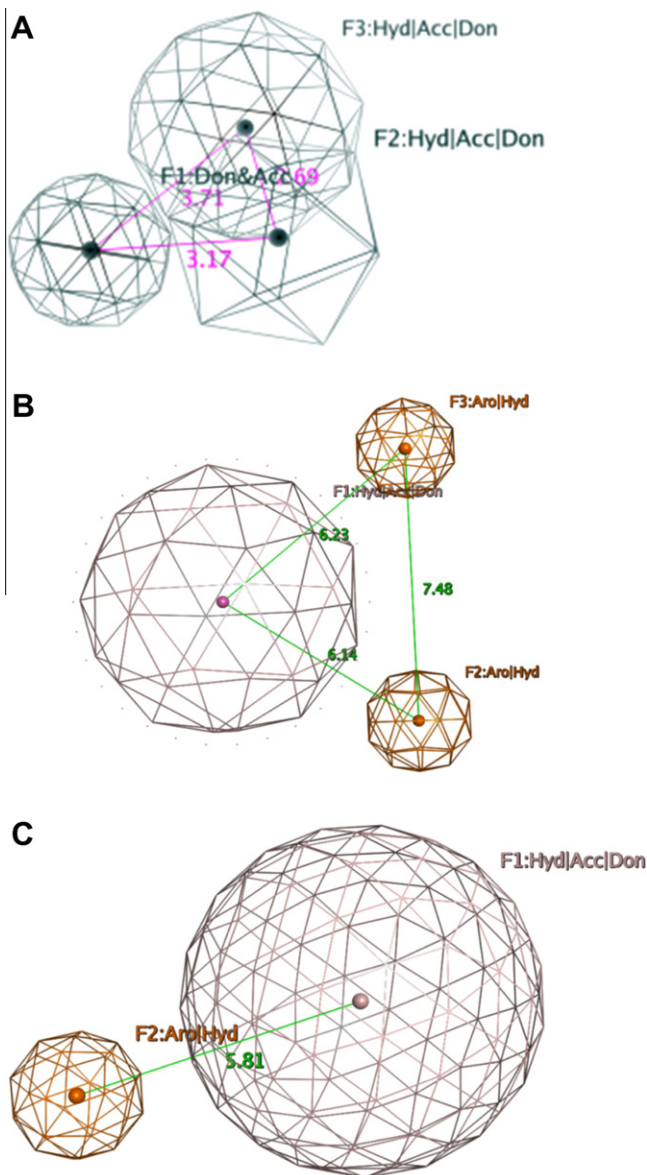
Figure 7. Pharmacophore contours and distances of the data set. (A) (2*R*, 3*R*, 4*S*)-2-aminomethylpyrrolidine 3,4-diol derivatives, (B) functionalized pyrrolidine derivatives and (C) combined data set.

3.4. Pharmacophore analysis

Pharmacophore analysis results obtained from the data set are graphically represented in Figure 7(a–c). In this study, two set of compounds carrying (2*R*, 3*R*, 4*S*)-2-aminomethylpyrrolidine 3,4-diol and functionalized pyrrolidine derivatives were flexi-aligned for the pharmacophore development. The Figure 7(a) provides pharmacophore of (2*R*, 3*R*, 4*S*)-2-aminomethylpyrrolidine 3,4-diol of derivatives, which has two hydrophobic/acceptor/donor (Hyd/Acc/Don) and one donor/acceptor (Don/Acc) contours. The pharmacophoric distances between the don/acc to the hyd/acc/don are 3.17 Å and 3.71 Å and the distance between both hyd/acc/don is 2.69 Å. The pharmacophore contours for the functionalized pyrrolidine derivative (Fig. 7b) and the combined data set (Fig. 7c) provided hyd/acc/don and aromatic/hydrophobic (Aro/Hyd) are the important contours and are separated by a distance >6 Å (6.14 Å and 6.23 Å) and <6 Å (5.81 Å) respectively. Also, the aro/hyd contours are separated by large distance (7.48 Å). These results reveal that the molecules should have hydrophobic region

away from the hydrophilic or the polar region of the molecules. The distributed hydrophobicity play important role to reduce/maintain the optimum polar property of the molecules. The aro/hyd property suggests that the active site of the enzyme possessed some aromatic or hydrophobic amino acids for the interactions.

4. Conclusion

This study concluded that the active sites of the α-mannosidase I and α-mannosidase II enzymes (from docking study) and the almond and jackbean α-mannosidase enzymes (from QSAR study) possess hydrophilic region (positively as well negatively) formed through acidic amino acids and the aromatic residues make a hydrophobic cavity, which interact with aromatic rings in the molecules. Therefore, the main interactions between all pyrrolidine derivative and both enzymatic classes (α-mannosidase enzymes I and II) occur by hydrogen bonds, hydrophobic π–π stacking contacts and salt bridges with the cation calcium and close interaction with zinc ion, respectively. The results derived from the QSAR analysis also reveal that the presence of polar property on the vdW surface of the molecules is important along with the presence of aromatic rings in the compounds. It suggests that the vdW surface properties play important role for the interaction of these molecules. The bond flexibility and number of rings in the molecules provide orientation of the aromatic groups for the hydrophobic π–π stacking contacts. The pharmacophore results derived from the analysis also support the abovementioned statement for the necessity of aromatic rings and polar properties for the inhibitory activity.

Herein, comprehensive molecular docking and QSAR studies on the binding mode of several pyrrolidine derivatives into the α-mannosidase active sites were performed. The results obtained indicate that the scoring function of AutoDock is adequate in predicting the correct binding modes of well known inhibitors in relation to their available X-ray structures. Subsequently, similar protocol was applied to correctly describe the binding mode of several pyrrolidine derivatives into the α-mannosidase active sites. Our results suggest that the best compound to inhibit both classes of α-mannosidase is the compound 30, which may be used to design similar and better inhibitors. Hence these analysis results such as QSAR and docking analysis provide active site characters of the α-mannosidase. Therefore, these findings are particularly relevant for the design of novel compounds and these structure-based approaches may lead to improved inhibitors for the next generation drugs.

Supplementary data

Supplementary data associated with this article can be found, in the online version, at http://dx.doi.org/10.1016/j.bmc.2012.10.011.

References and notes

1. Gamblin, D. P.; Scanlan, E. M.; Davis, B. G. *Chem. Rev.* **2009**, *109*, 131.
2. Park, H.; Hwang, K. Y.; Kim, Y. H.; Oh, K. H.; Lee, J. Y.; Kim, K. *Bioorg. Med. Chem. Lett.* **2008**, *18*, 3711.
3. Rawling, A. J.; Lomas, H.; Adam, W. P.; Marvin, J. R. L.; Dominic, S. A.; Shane, J. S. R.; Sarah, F. J.; George, W. J. F.; Raymond, A. D.; John, H. J.; Terry, D. B. *ChemBioChem* **2009**, *10*, 1101.

4. Shah, N.; Kuntzt, D. A.; Rose, D. R. *Proc. Natl. Acad. Sci. U.S.A.* **2008**, *105*, 9570.
5. Numao, S.; Kuntz, D. A.; Withers, S. G.; Rose, D. R. *J. Biol. Chem.* **2003**, *278*, 48074.
6. Scanlan, C. N.; Offer, J.; Zitzmann, N.; Dwek, R. A. *Nature* **2007**, *446*, 1038.
7. Vallee, F.; Karaveg, K.; Herscovics, A.; Moremen, K. W.; Howell, P. L. *J. Biol. Chem.* **2000**, *275*, 41287.
8. Tempel, W.; Karaveg, K.; Liu, Z. J.; Rose, J.; Wang, B. C.; Moremen, K. W. *J. Biol. Chem.* **2004**, *279*, 29774.
9. Karaveg, K.; Siriwardena, A.; Tempel, W.; Liu, Z. J.; Glushka, J.; Wang, B. C.; Moremen, K. W. *J. Biol. Chem.* **2005**, *280*, 16197.
10. Cantu, D.; Nerinckx, W.; Reilly, P. J. *Carbohydr. Res.* **2008**, *343*, 2235.
11. Sanap, S. S.; Ghosh, S.; Jabgunde, A. M.; Pinjari, R. V.; Gejji, S. P.; Singh, S.; Chopade, B. A.; Dhavale, D. D. *Org. Biomol. Chem.* **2010**, *8*, 3307.
12. Kumar, A.; Singhal, N. K.; Ramanujam, B.; Mitra, A.; Rameshwaram, N. R.; Nadimpalli, S. K.; Rao, C. P. *Glycoconjugate J.* **2009**, *26*, 495.
13. Moorthy, N. S. H. N.; Ramos, M. J.; Fernandes, P. A. *Lett. Drug Des. Discovery* **2011**, *8*, 14.
14. Moorthy, N. S. H. N.; Ramos, M. J.; Fernandes, P. A. *J. Enzyme Inhibit. Med. Chem.* **2012**, *27*, 649.
15. Moorthy, N. S. H. N.; Ramos, M. J.; Fernandes, P. A. *J. Enzyme Inhibit. Med. Chem.* **2011**, *26*, 78.
16. Moorthy, N. S. H. N.; Ramos, M. J.; Fernandes, P. A. *J. Enzyme Inhibit. Med. Chem.* **2011**, *26*, 755.
17. Moorthy, N. S. H. N.; Ramos, M. J.; Fernandes, P. A. *Med. Chem.* **2011**, *7*, 526.
18. Moorthy, N. S. H. N.; Ramos, M. J.; Fernandes, P. A. *Arch. Pharm.* **2012**, *345*, 265.
19. Brás, N. F.; Fernandes, P. A.; Ramos, M. J. *Theor. Chem. Acc.* **2009**, *122*, 283.
20. Brás, N. F.; Fernandes, P. A.; Ramos, M. J. *J. Chem. Theory Comput.* **2010**, *6*, 421.
21. Brás, N. F.; Ramos, M. J.; Fernandes, P. A. *J. Mol. Struct. (THEOCHEM)* **2009**, *946*, 125.
22. Brás, N. F.; Moura-Tamames, S. A.; Fernandes, P. A.; Ramos, M. J. *J. Comput. Chem.* **2008**, *29*, 2565.
23. Kuntz, D. A.; Zhong, W.; Guo, J.; Rose, D. R.; Boons, G. J. *ChemBioChem* **2009**, *10*, 268.
24. Kuntz, D. A.; Nakayama, S.; Shea, K.; Hori, H.; Uto, Y.; Nagasawa, H.; Rose, D. R. *ChemBioChem* **2010**, *11*, 673.
25. Englebienne, P.; Fiaux, H.; Kuntz, D. A.; Corbeil, C. R.; Gerber-Lemaire, S.; Rose, D. R.; Moitessier, N. *Proteins* **2007**, *69*, 160.
26. Sivapriya, K.; Hariharaputran, S.; Suhas, V. L.; Chandra, N.; Chandrasekaran, S. *Bioorg. Med. Chem.* **2007**, *15*, 5659.
27. Moorthy, N. S. H. N.; Ramos, M. J.; Fernandes, P. A. *Chemom. Intell. Lab Syst.* **2011**, *109*, 101.
28. Moorthy, N. S. H. N.; Cerqueira, N. M. F. S.; Ramos, M. J.; Fernandes, P. A. *Med. Chem. Res.* **2012**, *21*, 739.
29. Popowycz, F.; Gerber-Lemaire, S.; Demange, R.; Rodriguez-García, E.; Asenjo, A. T. C.; Robinab, I.; Vogel, P. *Bioorg. Med. Chem. Lett.* **2001**, *11*, 2489.
30. Fiaux, H.; Popowycz, F.; Favre, S.; Schutz, C.; Vogel, P.; Gerber-Lemaire, S.; Juillerat-Jeanneret, L. *J. Med. Chem.* **2005**, *48*, 4237.
31. van den Elsen, J. M.; Kuntz, D. A.; Rose, D. R. *EMBO J.* **2001**, *20*, 3008.
32. MOE, Chemical Computing Group: Montreal, H3A 2R7 Canada, 2007.
33. Lin, A. *J. Chem. Comput. Group* **2002**; http://www.chemcomp.com/Journal_of_CCG/Features/descr.htm.
34. Statistica 8.0 software, StatSoft; Tulsa, OK, USA, 2008.
35. Kiralj, R.; Ferreira, M. M. C. *J. Braz. Chem. Soc.* **2009**, *20*, 770.
36. Gramatica, P. *QSAR Comb. Sci.* **2007**, *26*, 694.
37. Moorthy, N. S. H. N.; Cerqueira, N. S.; Ramos, M. J.; Fernandes, P. A. *Med. Chem. Res.* **2012**, *21*, 133.
38. Gaussian. Carnegie Office Park, Bldg. 6, Pittsburgh, PA.
39. Cerqueira, N. M. F. S. A.; Ribeiro, J.; Fernandes, P. A.; Ramos, M. J. *Int. J. Quant. Chem.* **2011**, *111*, 1208.
40. Morris, G. M.; Goodsell, D. S.; Halliday, R. S.; Huey, R.; Hart, W. E.; Belew, R. K.; Olson, A. J. *J. Comput. Chem.* **1998**, *19*, 1639.
41. Humphrey, W.; Dalke, A.; Schulten, K. *J. Mol. Graphics* **1996**, *14*, 27.
42. Golbraikh, A.; Tropsha, A. *J. Mol. Graphics Modell.* **2002**, *20*, 269.
43. Moorthy, N. S. H. N.; Sousa, S. F.; Ramos, M. J.; Fernandes, P. A. *J. Enzyme Inhibit. Med. Chem.* **2011**, *26*, 777.
44. Moorthy, N. S. H. N.; Ramos, M. J.; Fernandes, P. A. *Curr. Drug Discov. Technol.* **2012**, *9*, 25.
45. Cook, R.; Dennis, J. *Am. Stat. Assoc.* **1979**, *74*, 169.
46. Moorthy, N. S. H. N.; Sousa, S. F.; Ramos, M. J.; Fernandes, P. A. *J. Biomol. Screen.* **2011**, *16*, 1037.
47. Moorthy, N. S. H. N.; Ramos, M. J.; Fernandes, P. A. *SAR QSAR Environ. Res.* **2012**, *23*, 521.
48. Durbin, J.; Watson, G. S. *Biometrika* **1950**, *37*, 409.
49. Durbin, J.; Watson, G. S. *Biometrika* **1951**, *38*, 159.
50. Cruciani, C.; Crivori, P.; Carrupt, P. A.; Testa, B. *J. Mol. Struct. (THEOCHEM)* **2000**, *503*, 17.
51. Moorthy, N. S. H. N.; Ramos, M. J.; Fernandes, P. A. *RSC Adv.* **2011**, *1*, 1126.
52. Gao, H. *J. Chem. Inf. Comput. Sci.* **2001**, *41*, 402.
53. Gonzalez, M. P.; Teran, C.; Teijeira, M.; Besada, P.; Gonzalez-Moa, M. J. *Bioorg. Med. Chem. Lett.* **2005**, *15*, 3491.
54. Oprea, T. I. *J. Comput. Aided Mol. Des.* **2000**, *14*, 251.
55. Labute, P. *J. Mol. Graphics Modell.* **2000**, *18*, 464.
56. Wildman, S. A.; Crippen, G. M. *J. Chem. Inf. Comput. Sci.* **1999**, *39*, 868.
57. Kumar, N. S.; Kuntz, D. A.; Wen, X.; Pinto, B. M.; Rose, D. R. *Proteins* **2008**, *71*, 1484.
58. Kawatkar, S. P.; Kuntz, D. A.; Woods, R. J.; Rose, D. R.; Boons, G. J. *J. Am. Chem. Soc.* **2006**, *128*, 8310.